Permeant-specific gating of connexin 30 hemichannels

Received for publication, July 7, 2017, and in revised form, September 28, 2017 Published, Papers in Press, October 5, 2017, DOI 10.1074/jbc.M117.805986

Brian Skriver Nielsen[‡1], **Jette Skov Alstrom**[‡], **Bruce J. Nicholson**[§], **Morten Schak Nielsen**[¶], **and Nanna MacAulay**[‡2]

From the [‡]*Center for Neuroscience and* [¶]*Department of Biomedical Sciences, Faculty of Health and Medical Sciences, University of Copenhagen, 2200 Copenhagen N, Denmark, and the* [§]*Department of Biochemistry, School of Medicine, University of Texas Health Science Center, San Antonio, Texas 78229*

Edited by Karen G. Fleming

Gap junctions confer interconnectivity of the cytoplasm in neighboring cells via docking of two connexons expressed in each of the adjacent membranes. Undocked connexons, referred to as hemichannels, may open and connect the cytoplasm with the extracellular fluid. The hemichannel configuration of connexins (Cxs) displays isoform-specific permeability profiles that are not directly determined by the size and charge of the permeant. To further explore Ca^{2+}-mediated gating and permeability features of connexin hemichannels, we heterologously expressed Cx30 hemichannels in *Xenopus laevis* oocytes. The sensitivity toward divalent cation-mediated gating differed between small atomic ions (current) and fluorescent dye permeants, indicating that these permeants are distinctly gated. Three aspartate residues in Cx30 (Asp-50, Asp-172, and Asp-179) have been implicated previously in the Ca^{2+} sensitivity of other hemichannel isoforms. Although the aspartate at position Asp-50 was indispensable for divalent cation-dependent gating of Cx30 hemichannels, substitutions of the two other residues had no significant effect on gating, illustrating differences in the gating mechanisms between connexin isoforms. Using the substituted cysteine accessibility method (SCAM), we evaluated the role of possible pore-lining residues in the permeation of ions and ethidium through Cx30 hemichannels. Of the cysteine-substituted residues, interaction of a proposed pore-lining cysteine at position 37 with the positively charged compound [2-(trimethylammonium)ethyl] methane thiosulfonate bromide (MTSET) increased Cx30-mediated currents with unperturbed ethidium permeability. In summary, our results demonstrate that the permeability of hemichannels is regulated in a permeant-specific manner and underscores that hemichannels are selective rather than non-discriminating and freely diffusable pores.

Gap junctions confer interconnectivity of the cytoplasm of neighboring cells via docking of two connexons, expressed in each of the adjacent membranes (1). Six connexins are required to produce the pore-forming connexon, and 21 distinct human connexin isoforms have been cloned and named according to their molecular mass in kDa (2). Gap junctions are permeable to a range of ions, second messengers, metabolites, etc., although they display distinct permeability profiles and preferences, depending on their isoform composition (3, 4). The distinct permeability profile is not simply related to permeant size and charge (3, 5), *i.e.* Cx32 gap junctions transfer adenosine (267 Da, no charge) and inositol 1,4,5-trisphosphate (IP_3) (420 Da, six negative charges) 12- and 2.5-fold more efficiently than Cx43 gap junctions, whereas Cx43 gap junctions are 18-fold more permeable to AMP (347 Da, two negative charges) and ADP (427 Da, three negative charges) (6–8). We have also observed that Cx43 gap junctions show 20-fold differences in permeability compared with AMP and cAMP, which differ by a single phosphodiester bond.[3] Regulation of the permeation of ions *versus* larger fluorescent dyes through gap junctions is also not always proportional (9, 10), as factors such as phosphorylation by protein kinase C have been seen to affect ion currents and dye permeation differently (11).

Connexons located in a plasma membrane may, in the absence of an adjacent partner, act as a hemichannel; that is, serve as a channel connecting the cytoplasm with the extracellular fluid. Opening of hemichannels has been proposed to occur by a range of diverse molecular cues, such as removal of divalent cations (12–15), metabolic inhibition (16–18), membrane potentials more positive than +40 mV (in the case of Cx43 (19, 20)), membrane stretch (21, 22), and exposure to cytokines or growth factors (23, 24). Hemichannel activity is routinely investigated with uptake of fluorescent probes (14, 17, 25, 26), and it has been inferred that this reflects permeability to biologically relevant substrates of sizes below that of the fluorescent probe (14, 16, 18, 27). We recently documented that Cx43 hemichannel–mediated uptake of a fluorescent probe did not serve as a proportional readout of permeability toward a range of smaller biological molecules, such as glutamate, glutathione, glucose, lactate, atomic ions (current), mannitol, glycerol, and urea (20, 28). The hemichannels therefore do not act as open aqueous pores allowing non-selective free diffusion of permeants below 500 Da. Although removal of divalent cations promoted a robust Gd^{3+}-sensitive ethidium uptake in Cx43-expressing oocytes with no detectable Cx43-mediated current, removal of divalent cations promoted Gd^{3+}-sensitive ethidium uptake and membrane currents in Cx30-expressing oocytes (20, 28). These findings show that connexin hemichannels, by analogy with gap junctions, display isoform-specific permeabil-

This work was predominantly supported by the Faculty of Health and Medical Sciences (University of Copenhagen). The authors declare that they have no conflicts of interest with the contents of this article.

[1] Supported by the Faculty of Health and Medical Sciences (University of Copenhagen).

[2] To whom correspondence should be addressed: University of Copenhagen, Blegdamsvej 3, 2200 Copenhagen N, Denmark. Tel.: 45-35327566; E-mail: macaulay@sund.ku.dk.

[3] M. Toloue, J. Nitsche, and B. J. Nicholson, unpublished results.

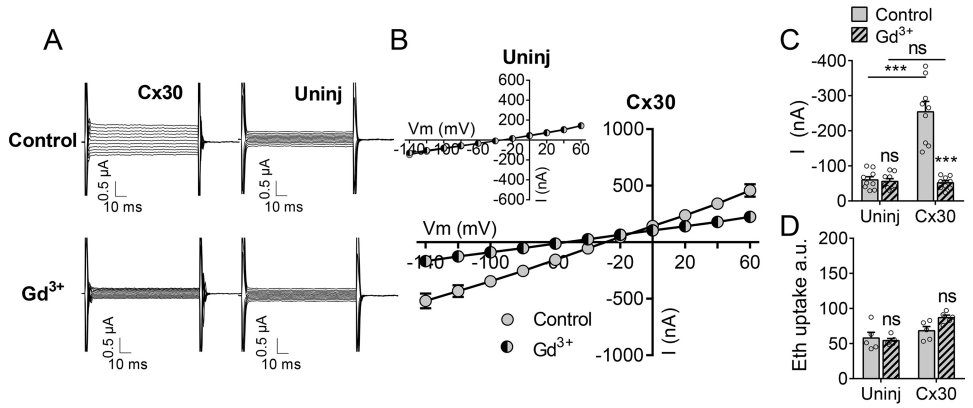

Figure 1. Activity of Cx30 hemichannels at physiological divalent cation concentrations. *A*, membrane currents were recorded by application of 100-ms voltage steps from +60 to −140 mV in steps of 20 mV from a holding potential of −50 mV in oocytes exposed to control solution (*top panels*) and after 1-min exposure to control solution containing 50 μM Gd^{3+} (*bottom panels*). *Uninj*, uninjected. *B*, summarized I/V curves for Cx30-expressing oocytes ($n = 9$) and uninjected oocytes ($n = 9$, *inset*). *C*, histogram of currents obtained at −80 mV in control solution ($n = 9$) and control solution containing 50 μM Gd^{3+} ($n = 9$). *D*, ethidium uptake recorded after 60-min exposure to control solution ($n = 5$) or control solution containing 50 μM Gd^{3+} ($n = 5$). Data in I/V curves and in the bar graphs are presented as mean ± S.E. The individual data points are shown by overlaid scatterplots in bar graphs. Statistical significance was tested using repeated measures two-way ANOVA with Bonferroni post hoc test and marked by *asterisks above the columns* when comparing control and Gd^{3+} within the two groups and with *asterisks above the horizontal lines* when comparing between the two groups. ***, $p < 0.001$; *ns*, not significant.

ity profiles that are not simply dictated by size and charge. It is, however, uncertain whether the permeability toward diverse permeants is differentially regulated, as reported for gap junctions (29). We therefore set out to determine the regulation of Cx30-mediated hemichannel permeability toward a fluorescent probe *versus* atomic ions (current). For this purpose, we assessed Cx30 hemichannel activity upon expression in *Xenopus laevis* oocytes, which display negligible functional expression of other endogenous large-pore channels and thus allow biophysical characterization of Cx30 in isolation.

Results

The gating of Cx30 hemichannels by divalent cations depends on the permeant

To determine whether the Cx30-dependent permeation of atomic ions (current) and fluorescent dye responds proportionately to gating by divalent cations, we expressed Cx30 in *Xenopus* oocytes. This heterologous expression system has the inherent advantage of low expression of endogenous proteins with overlapping activation, inhibition, and/or permeability profiles. In control solution (which, for frog Ringer's solution, contains 1 mM Ca^{2+} and 1 mM Mg^{2+}), the membrane current was 3-fold larger in oocytes expressing Cx30 than that observed in uninjected oocytes (representative current traces, Fig. 1*A*; I/V[4] curves, Fig. 1*B*; membrane currents obtained at $V_m = -80$ mV, Fig. 1*C*). The connexin hemichannel inhibitor gadolinium (Gd^{3+}) had no effect on membrane currents of uninjected control oocytes (Fig. 1, *A*, *B* (inset), and *C*) but decreased membrane currents in oocytes expressing Cx30 to close to that of uninjected oocytes (Fig. 1, *A*–*C*). Cx30-expressing oocytes thus permit Gd^{3+}-sensitive membrane currents in the presence of 1 mM each of the divalent cations. In contrast, batch-matched oocytes kept in control solution displayed no Cx30-mediated Gd^{3+}-sensitive ethidium uptake (Fig. 1*D*), indicating that the basal concentration of divalent cations (1 mM) suffices to prevent ethidium permeability through Cx30 even though it does not fully block ionic conductance.

To determine the individual gating by the two divalent cations (Ca^{2+} and Mg^{2+}) on Cx30-mediated conductance and ethidium uptake, we exposed the oocytes to solutions free of Mg^{2+} (MgFS), free of Ca^{2+} (CaFS), or free of both divalent cations (DCFS). Membrane currents in uninjected control oocytes were not significantly affected by removal of either of the divalent cations or both divalent cations (Fig. 2, *A*, *B*, and *D*). In Cx30-expressing oocytes, selective removal of Mg^{2+} had no effect on Cx30-mediated membrane currents, whereas selective removal of Ca^{2+} caused a 4-fold increase in membrane currents (Fig. 2, *A*, representative current traces; *C*, I/V curves; and *D*, summarized data at −80 mV). This current was further augmented (to 10-fold of control) by removal of both divalent cations, and sensitive to Gd^{3+} (Fig. 2, *A*, *C*, and *D*). In comparison, selective removal of Ca^{2+} did not significantly affect Cx30-mediated ethidium uptake, and ethidium uptake was only increased (by 5-fold) over that of the control situation when both divalent cations were removed, in a Gd^{3+}-sensitive manner (Fig. 2*E*). As expected, ethidium uptake in uninjected oocytes was unaffected by the extracellular concentration of divalent cations and insensitive to Gd^{3+} (Fig. 2*E*). These results suggest that the Ca^{2+} sensitivity differs between Cx30-mediated current and ethidium permeability.

The Ca^{2+} and Mg^{2+} sensitivity of the hemichannel current and ethidium uptake was more rigorously examined by determination of the IC_{50} for each divalent cation in the complete absence of the other for both ethidium uptake and membrane currents. The IC_{50} for Ca^{2+} was 4.5-fold lower for ethidium uptake than for the membrane currents (49 ± 8 μM, $n = 5$ for ethidium uptake *versus* 228 ± 37 μM, $n = 9$ for membrane current, $p < 0.01$) (Fig. 3*A*). Similarly, the IC_{50} for Mg^{2+} was 3.5-fold lower for ethidium uptake than for the membrane currents (179 ± 26 μM, $n = 5$ for ethidium uptake *versus* 635 ± 123

[4] The abbreviations used are: I/V, voltage/current; MgFS, magnesium-free solution; CaFS, calcium-free solution; DCFS, divalent cation–free solution; SCAM, substituted cysteine accessibility method; MTS-ET, [2-(trimethylammonium)ethyl] methane thiosulfonate bromide; MTS-ES, sodium (2-sulfonatoethyl) methane thiosulfonate; KID, keratitis ichthyosis deafness; ANOVA, analysis of variance.

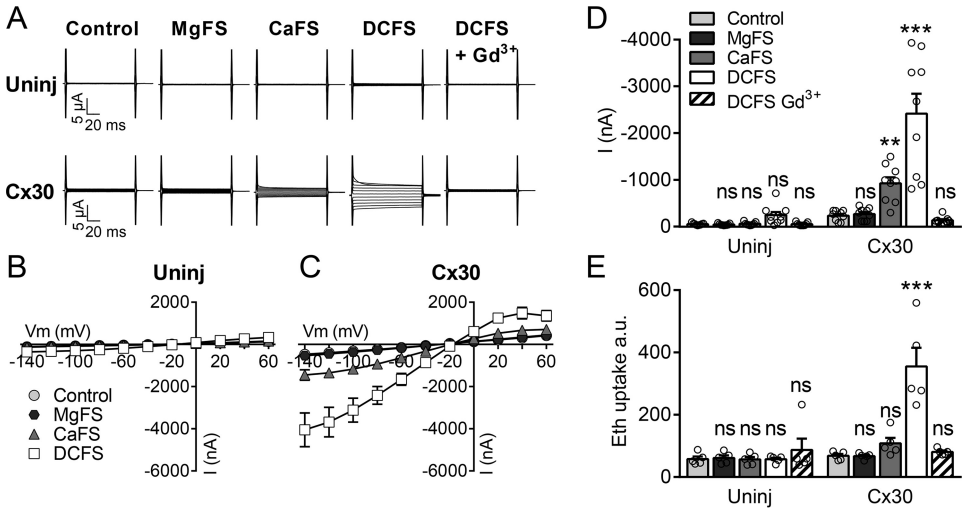

Figure 2. Effect of divalent cations on Cx30 hemichannel activity. *A*, membrane currents were recorded on uninjected (*Uninj*) oocytes (*top row*) or Cx30-expressing oocytes (*bottom row*) during application of 100-ms voltage steps from +60 to −140 mV in steps of 20 mV from a holding potential of −50 mV. Membrane currents were recorded in control solution and after 1-min exposure to MgFS, CaFS, DCFS, and DCFS containing 50 μM Gd^{3+} in random order. *B* and *C*, summarized I/V curves are illustrated for uninjected oocytes (*B*, $n = 9$) and Cx30-expressing oocytes (*C*, $n = 9$). *D*, histogram of currents obtained at −80 mV. *E*, ethidium uptake after 60-min exposure to control solution, MgFS, CaFS, DCFS, or DCFS containing 50 μM Gd^{3+} ($n = 5$). Data in I/V curves and in the bar graphs are presented as mean ± S.E. The individual data points are shown by overlaid scatterplots in bar graphs. Statistical significance was tested using repeated measures two-way ANOVA with Bonferroni post hoc test. **, $p < 0.01$; ***, $p < 0.001$; *ns*, not significant.

μM, $n = 12$ for membrane current, $p < 0.05$) (Fig. 3*B*). Given that all measurements occurred within the linear response range of the system for detection of both dye and current, these differences indicate that Ca^{2+} and Mg^{2+} have distinguishable effects on the permeability of Cx30 hemichannels to current and larger permeants.

Amino acids important for calcium sensitivity

The Ca^{2+} sensitivity of connexin hemichannels are proposed to be conferred via extracellular aspartate residues, which bind Ca^{2+} with high affinity (30). Three aspartate residues, implicated in regulating the calcium sensitivity of other connexin hemichannels (31–34), correspond to Asp-50, Asp-172, and Asp-179 in Cx30 (Fig. 4*A*). The role of these aspartate residues in calcium sensitivity of Cx30 hemichannels was tested by individually mutating each to asparagine, which is similar in size but lacks the negative charge of the aspartates and, thus, the ability to coordinate calcium binding. Oocytes expressing the Cx30-D50N mutation consistently lysed (Fig. 4*B*), even when stored in solution containing 10 mM Ca^{2+} (data not shown), indicating lack of Ca^{2+}-dependent gating and, thus, continuous ion leakage through the hemichannel pore. We observed a sizeable ATP release from the Cx30-D50N–expressing oocytes when investigated <24 h after microinjection of the RNA encoding this channel (Fig. 4*C*). Although this was prior to visible cell lysis, the degree to which the membrane may have been compromised during this initial period could not be assessed. Membrane currents and ethidium uptake were not significantly affected by the removal of divalent cations from uninjected oocytes (Fig. 4, *D*, *H*, and *I*) but were both readily observed in DCFS in oocytes expressing the WT (Fig. 4, *E*, *H*, and *I*) and the mutant Cx30 constructs Cx30-D172N (Fig. 4, *F*, *H*, and *I*) or Cx30-D179N (Fig. 4, *G*–*I*). For all constructs, the membrane current activity and ethidium uptake were nearly abolished by 1 mM and 5 mM Ca^{2+} in the test solutions (Fig. 4, *H* and *I*). Despite consistent observation of DCFS-sensitive current and dye uptake in oocytes expressing WT Cx30 and the mutant versions (D172N and D179N), no DCFS-dependent ATP release was detected using a luciferase assay (Fig. 4*J*). The functionality of the assay was confirmed by measurement of total ATP content by oocyte lysis at the termination of the experiment (Fig. 4, *C* and *J*). Thus, aspartate in position 50 is required for Ca^{2+}-dependent gating of Cx30 hemichannels, whereas the aspartate residues at position 172 and 179 are of minor, if any, importance for divalent cation–dependent gating of both current and ethidium uptake through Cx30. Furthermore, data show that, although removal of divalent cations opens Cx30 to ethidium and current, it does not, under our experimental conditions, confer detectable permeability to ATP, as has been reported for other hemichannels.

Probing of the Cx30 pore with cysteine-interacting thiol reagents

To evaluate the role of possible pore-lining residues in permeation of atomic ions *versus* ethidium through Cx30 hemichannels, we employed the substituted cysteine accessibility method (SCAM). This is an established experimental approach to determine pore-lining residues (35, 36) where individual residues are mutated to cysteines. Their accessibility to the aqueous environment (*e.g.* by exposure to the conductive pore) is then measured by reactivity with membrane-impermeable thiol reagents added from the extracellular medium, which can affect the permeation pathway through the pore. Select amino acids in Cx30, identified to be pore-lining in other connexin isoforms (35–42), were substituted with cysteine to generate: Cx30-V37C, E42C, V84C, Y136C, I145C, and F150C (Fig. 5*A*). The equivalent positions to Val-37 and Glu-42 in M1/E1 are in the pore in the X-ray structure of Cx26 (37), and Glu-42 was reactive in SCAM analysis of Cx46 hemichannels (35, 39).

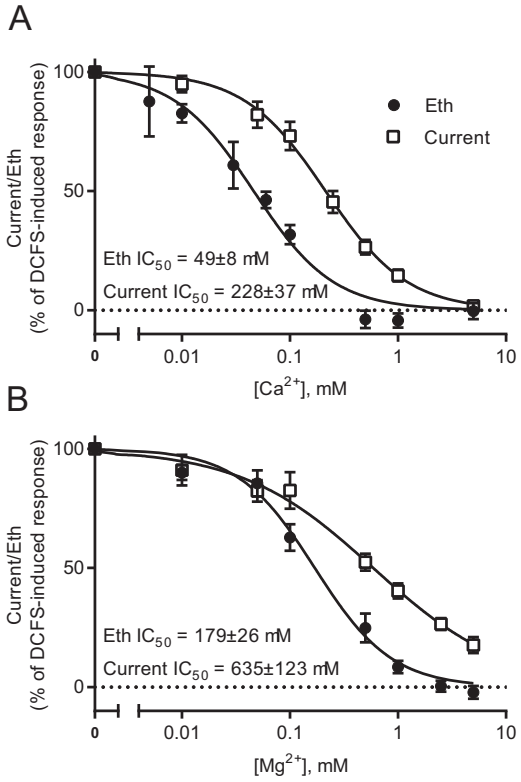

Figure 3. Cx30 hemichannel gating of currents *versus* ethidium uptake by divalent cations. *A* and *B*, membrane currents were recorded in Cx30-expressing oocytes by application of 100-ms voltage steps from +60 to −140 mV in steps of 20 mV from a holding potential of −50 mV. The currents recorded at −80 mV were used for further analysis. The membrane currents were recorded after exposure to different concentrations of Ca^{2+} (*A*, $n = 9$) or Mg^{2+} (*B*, $n = 12$) in random order for 1 min. Between each test solution, the oocytes were exposed to control solution until the current returned to baseline. After exposure to eight different concentrations of Ca^{2+} (*A*) or Mg^{2+} (*B*), the membrane currents were recorded after 1-min exposure to 5 mM Ca^{2+} (*A*) or Mg^{2+} (*B*) containing 50 μM Gd^{3+}. Ethidium (*Eth*) uptake was determined after 60-min exposure to (*A*) different concentrations of Ca^{2+} or 5 mM Ca^{2+} containing 50 μM Gd^{3+} or (*B*) different concentrations of Mg^{2+} or 5 mM Mg^{2+} containing 50 μM Gd^{3+} ($n = 5$). For both membrane currents and ethidium uptake, 100% activity was determined in divalent cation–free solution, and 0% activity was determined in 5 mM Ca^{2+} (*A*) or Mg^{2+} (*B*) containing 50 μM Gd^{3+}. The normalized data were fitted by nonlinear regression analysis with a variable slope Y = 100/(1 + 10^((logIC_{50} − X) × Hill slope)), where X is the logarithm of the concentration, to obtain the IC_{50}, and statistical significance was tested with unpaired *t* test. Data in I/V curves are presented as mean ± S.E.

Val-84 in M2 and Tyr-136, Ile-145, and Phe-150 in M3 were all mapped to the Cx32 gap junction pore by SCAM (36, 42).

These mutated forms of Cx30 all expressed robustly at the plasma membrane fraction of cRNA-injected *Xenopus* oocytes (Fig. 5*B*). However, only two of the Cx30 mutants (Cx30-V37C and Cx30-I145C) displayed functional hemichannel activity, as recorded by Gd^{3+}-sensitive DCFS-induced membrane currents (Fig. 5, *C*, representative current traces; *D* and *E*, summarized I/V curves; and *F*, currents obtained at −80 mV) and ethidium uptake (Fig. 5*G*). Prior to thiol reactivity testing, we verified that WT Cx30 hemichannel activity and its sensitivity to removal of divalent cations were unaffected by addition of the cationic thiol reagent MTS-ET (molecular mass, 278 Da) (Fig. 6, *A* and *D*). Ethidium uptake in Cx30-expressing oocytes was also not affected by addition of MTS-ET and remained sensitive to removal of divalent cations (Fig. 6*E*). Thus, any effects of MTS-ET on a cysteine mutant can be reliably assigned to an interaction with the mutated residue.

Of the two functional cysteine mutants tested, MTS-ET did not affect currents of Cx30-I145C (Fig. 6, *C* and *D*) but more than doubled the current through Cx30-V37C in the presence of divalent cations (Fig. 6, *B* and *D*). Both mutant constructs retained their DCFS-induced enhancement of the current after treatment with MTS-ET (Fig. 6, *B–D*), which also remained Gd^{3+}-sensitive (data not shown). Time control experiments without MTS-ET addition verified that the altered current observed in Cx30-V37C– expressing oocytes was in fact due to addition of the MTS-ET reagent and did not occur as a simple function of time ($n = 10$, data not shown). In contrast, ethidium uptake in oocytes expressing Cx30-V37C or Cx30-I145C was unaffected by MTS-ET treatment, although both mutant versions of Cx30 remained sensitive to DCFS after MTS-ET treatment (Fig. 6*E*). In summary, residue 145 was either inaccessible to the MTS-ET reagent or the reaction did not affect pore permeability to ethidium or ions. In contrast, the MTS-ET reaction at residue 37, although not preventing opening of the pore in the absence of extracellular divalent cations, significantly increased current in the presence of divalent cations, with no concomitant change in ethidium permeability.

To assess whether there is a possible charge dependence of the thiol reagent, a parallel experimental series was carried out with the anionic membrane-impermeable reagent MTS-ES (molecular mass, 242 Da). MTS-ES also had no effect on WT Cx30 hemichannel-mediated currents or ethidium uptake in control solution, and the hemichannels remained sensitive to DCFS (Fig. 7, *A*, *D*, and *E*). In contrast to the cationic thiol, MTE-ES also had no effect on any of the tested transport parameters for either of the mutant constructs (Fig. 7, *B–E*), indicating that either the anionic thiol does not gain access to the hemichannel pore, is unreactive with the tested sites, or did not affect the pore properties upon reaction.

Discussion

This study demonstrates that the divalent cation–mediated gating of the Cx30 hemichannel pore depends on the nature of the tested permeant. The results support the notion that open connexin hemichannels do not represent freely permeable nonselective pores and that the specific permeability profile of each hemichannel can be modulated by external factors in such a manner that a permeability profile determined in one setting may not apply to another setting.

For reasons of technical ease, connexin hemichannel activity is commonly determined by use of fluorescent dye permeability (14, 43). Connexin hemichannel–mediated dye uptake/release has typically been inferred to represent uptake/release of other molecules of similar or smaller molecular weight. In recent comprehensive biophysical studies, we established that connexin hemichannels are permeable to select permeants in an isoform-specific manner and that fluorescent dye uptake cannot be used as an indicator of permeability to other smaller solutes (Refs. 20, 28; for a review, see Ref. 45). Although Cx26 and Cx43 in their hemichannel configuration were rather restrictive in their permeability profile, Cx30 hemichannels were permeable to both atomic ions and ethidium upon

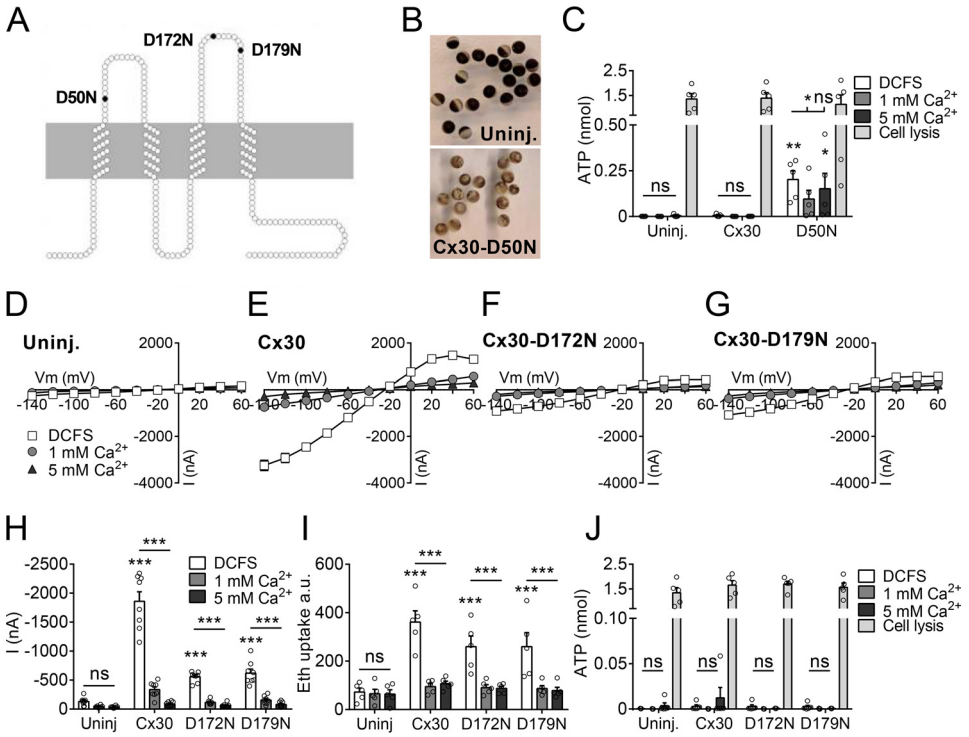

Figure 4. The role of Asp-50, Asp-172, and Asp-179 in Cx30 Ca^{2+} sensitivity. *A*, illustration of the three aspartate residues mutated to asparagine in Cx30 (D50N, D172N, and D179N). *B*, representative pictures of uninjected (*Uninj.*) oocytes and oocytes expressing the Cx30-D50N mutation in Kulori incubation medium (3 days after microinjection). *C*, determination of ATP release from uninjected oocytes, Cx30-expressing, or Cx30-D50N–expressing oocytes (<24 h after microinjection) after 60-min exposure to the different Ca^{2+} concentrations and after cell lysis at the termination of the experiment ($n = 5$). *D–G*, I/V curves from recorded membrane currents on uninjected oocytes, Cx30-expressing, Cx30-D172N–expressing, or Cx30-D179N–expressing oocytes by application of 200-ms voltage steps from −140 mV to +60 mV in increments of 20 mV from a holding potential of −30 mV ($n = 8$). Membrane currents were recorded after 1-min exposure to the different Ca^{2+} concentrations. *H*, summarized membrane currents obtained at −80 mV. *I*, ethidium uptake measured after 60-min exposure to different Ca^{2+} concentrations ($n = 5$). *J*, determination of ATP release from uninjected oocytes or Cx30-expressing, Cx30-D172N–expressing, or Cx30-D179N–expressing oocytes after 60-min exposure to the different Ca^{2+} concentrations and after cell lysis at the termination of the experiment ($n = 5$). Data in I/V curves and in the bar graphs are presented as mean ± S.E. The individual data points are shown by overlaid scatterplots in bar graphs. Statistical significance of total ATP content by oocyte lysis and DCFS-induced hemichannel activity was tested with one-way ANOVA with Dunnett's post hoc test (against Uninj-DCFS) and is marked by *asterisks above the columns* when significant. Statistical significance of Ca^{2+} sensitivity was tested using repeated measures two-way ANOVA with Bonferroni post hoc test and is marked by *asterisks above the horizontal lines*. *, $p < 0.05$; **, $p < 0.01$; ***, $p < 0.001$; *ns*, not significant.

removal of divalent cations from the test solution (28). The latter isoform therefore served as an ideal candidate to compare how gating affects different permeants. Differential regulation of ionic and metabolite permeability may have physiological significance. The studies were carried out with heterologous expression in *Xenopus* oocytes to obtain an experimental scenario in which the Cx30 hemichannels could be studied in isolation. *Xenopus* oocytes efficiently express ectopic proteins such as connexins and generally produce functional membrane channels with properties similar to those expressed by mammalian cells. However, we cannot exclude that certain binding partners are missing, that the lipid bilayer composition varies from that of mammalian cells and could modify properties, and/or that the phosphorylation pattern is altered in a manner affecting the permeability profile of the expressed protein.

In physiological solutions containing the basal concentrations (1 mM) of Ca^{2+} and Mg^{2+}, Cx30-expressing oocytes displayed significantly larger (Gd^{3+}-sensitive) basal membrane currents than those of the uninjected oocytes, whereas no differences in ethidium uptake could be detected. Currents, but not ethidium uptake, were further enhanced by selective removal of Ca^{2+} but not Mg^{2+}. The molecular basis for these observations became evident when the Ca^{2+} and Mg^{2+} responses of Cx30 channels were titrated with regard to both conductance and ethidium uptake. The IC_{50} for conductance was ~4-fold higher than that for ethidium uptake for both Ca^{2+} and Mg^{2+}. The IC_{50} values were ~3-fold higher for Mg^{2+} than for Ca^{2+}, whether tested for Cx30-mediated current or ethidium uptake. As the Cx30-mediated currents are well within the detection range for the two-electrode voltage clamp, and the ethidium uptake was measured in the linear part of the time-dependent flux (20), we can exclude that saturation of one or the other underlies the permeant-specific shifts in IC_{50}. These data support the initial observation that Ca^{2+} is the more potent stabilizer of the closed state of the connexin hemichannel, as also reported in the analysis of Cx26-mediated peak tail currents (46), and that the concentration of divalent cations required to close the hemichannel depends on the permeant.

Several possibilities exist for how the gating with respect to larger dyes may require lower concentrations of divalent cations. It is possible that there are two stages in channel gating as divalent cation concentration increases, initially to a residual state that prevents dye permeability but allows ion passage and, subsequently, to a fully closed state. However, this has not been specifically seen in single-channel recordings of Ca^{2+}-mediated gating of other hemichannels. An alternative possibility is suggested by the recent structure of the Cx26 channel in Ca^{2+} bound and free states, which concludes that, rather than chan-

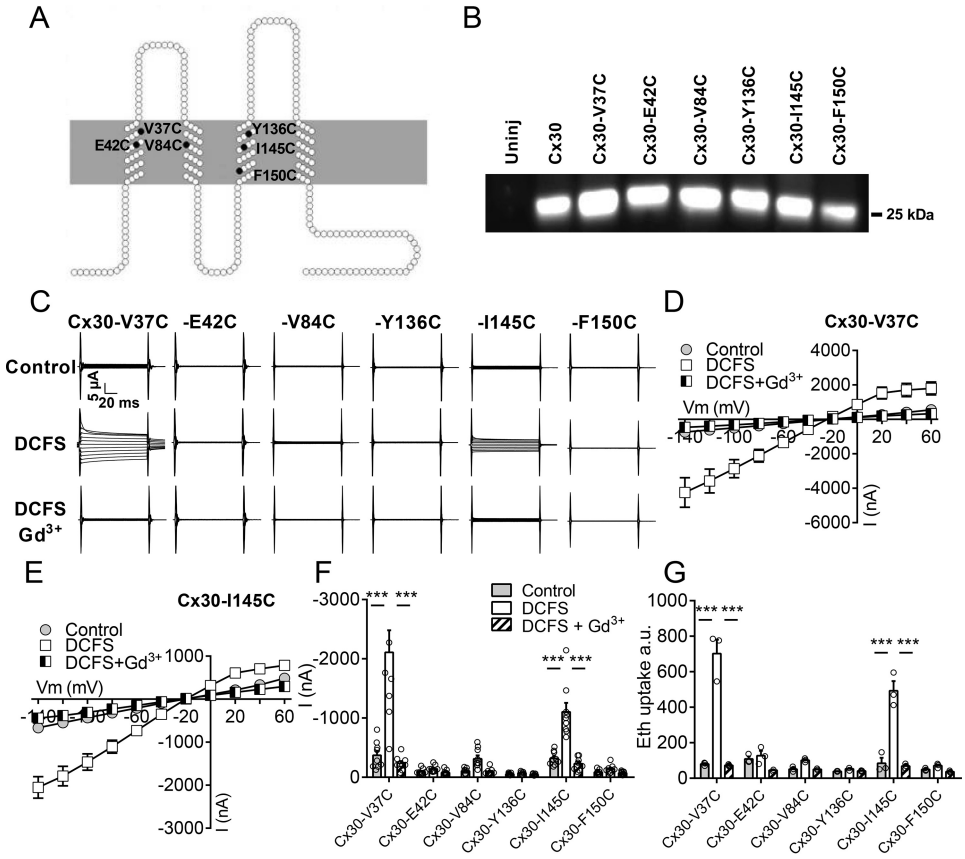

Figure 5. Functionality of cysteine-mutated Cx30 hemichannels. *A*, diagram of the six residues in Cx30 that were individually mutated to cysteine (Cx30-V37C, Cx30-E42C, Cx30-V84C, Cx30-Y136C, Cx30-I145C, and Cx30-F150C). *B*, plasma membranes were purified from uninjected (*uninj*) oocytes, oocytes expressing Cx30, or one of the six mutated forms of Cx30, subjected to SDS gel electrophoresis, and immunoblotted with anti-Cx30 antibodies. *C*, membrane currents were recorded on oocytes expressing the mutated Cx30 hemichannels in control solution after 1-min exposure to DCFS and DCFS containing 50 μM Gd^{3+}. Membrane currents were recorded by application of 100-ms voltage steps from +60 to −140 mV in steps of 20 mV from a holding potential of −50 mV. *D* and *E*, summarized I/V curves are illustrated for Cx30-V37C– expressing oocytes (*D*, $n = 9$) and Cx30-I145C (*E*, $n = 9$). *F*, histogram of currents obtained at −80 mV ($n = 9$). *G*, ethidium uptake recorded after 60-min exposure to control solution, DCFS, or DCFS containing 50 μM Gd^{3+} ($n = 3$). Data in I/V curves and in the bar graphs are presented as mean ± S.E. The individual data points are shown by overlaid scatterplots in bar graphs. Statistical significance was tested using repeated measures two-way ANOVA with Bonferroni post hoc test. ***, $p < 0.001$.

nel constriction, Ca^{2+} induces a change in the pore lining from a mix of anionic and cationic domains to a fully positive potential across the whole length of the pore (47). This is likely to have a much greater inhibitory effect on the passage of larger cations than smaller atomic cations through the pore. In addition, our preliminary studies indicate that Cx30 channels are not very ion-selective, so some current could still be carried by anions even with the highly positive potentials in the pore induced by Ca^{2+}.

In terms of the Ca^{2+} gating sites in Cx30, Asp-50 appears to be indispensable for Ca^{2+}-dependent closure of Cx30 hemichannels, as the oocytes expressing the mutated construct, Cx30-D50N, lysed even in the presence of high concentrations of Ca^{2+} in the incubation medium. This repeatedly observed cell lysis indicates that the mutated channel is unable to bind Ca^{2+} and, therefore, is constitutively open, with an ensuing continuous ion flux across the plasma membrane. We observed a robust ATP release from the Cx30-D50N– expressing oocytes, although it is unresolved whether this ATP exits through the pore of the mutated connexin or whether it is the result of the early stages of oocyte lysis. The equivalent mutation in Cx26 leads to keratitis ichthyosis deafness (KID) syndrome (48), although, in this case, Ca^{2+} sensitivity was simply reduced (49, 50), as high Ca^{2+} concentration in the incubation medium rescued oocytes expressing the Cx26-D50N mutant (31). The amino acids homologous to Cx30–Asp-172 and Cx30–Asp-179 in Cx32 have also been implicated in binding Ca^{2+} (34): mutation of either abolished the majority of the Ca^{2+}-dependent gating in Cx32 (34), and mutation of the latter site is associated with X-linked Charcot–Marie–Tooth disease (34, 51). However, in Cx30, mutation of these sites had no effect on the Ca^{2+}-mediated gating, indicating that the amino acid residues coordinating the Ca^{2+} ions in the different connexin isoforms may not be identical and that this isoform-specific manner of gating is yet another molecular differentiation between the connexin isoforms. Mutations may, however, be misleading, as they could influence any part of the gating pathway. In fact, Cx26-D50 has been implicated by molecular modeling, supported by cycle mutagenesis, to be more important for stabilization of a salt bridge with Lys-61 (49), whereas Glu-42, Glu-47, and the carbonyl of Gly-45 are implicated as the Ca^{2+}-binding site in the recent structure of the Ca^{2+}-bound form of Cx26 (47).

We were unable to detect DCFS-mediated ATP release by oocytes expressing Cx30 WT or the D172N or D179N mutant constructs with a luciferase assay. We have previously detected

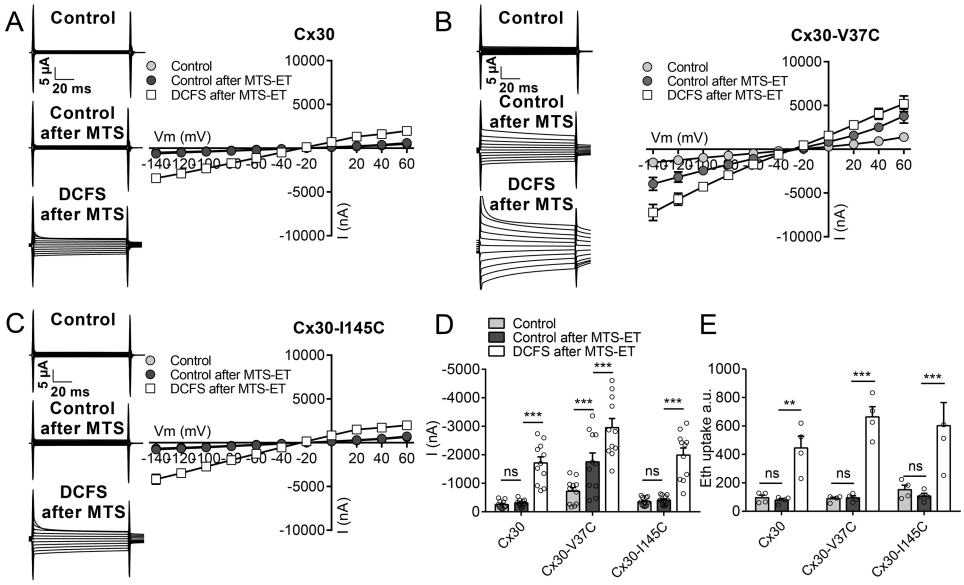

Figure 6. Effect of MTS-ET on Cx30, Cx30-V37C, and Cx30-I145C hemichannel activity. *A–C*, the effect of 1 min exposure to MTS-ET in control solution on the membrane currents was determined for Cx30 (*A*, $n = 11$), Cx30-V37C (*B*, $n = 11$), and Cx30-I145C (*C*, $n = 11$) hemichannels. Membrane currents were recorded by application of 100-ms voltage steps from +60 to −140 mV in steps of 20 mV from a holding potential of −50 mV. I/V relations were obtained in control solution and following exposure to MTS-ET in control solution for 1 min. Finally, the membrane currents were determined after 1-min exposure to DCFS. Representative current traces are shown in the *left panels*, and I/V summaries of $n = 11$ are shown in the *right panels*. *D*, histogram of all membrane currents obtained at −80 mV. *E*, ethidium (*Eth*) uptake recorded after 1-h exposure to control solution or DCFS after 5 min pretreatment in control solution or control solution containing 2 mM MTS-ET ($n = 4$ for all conditions). Data in I/V curves and in the bar graphs are presented as mean ± S.E. The individual data points are shown by overlaid scatterplots in bar graphs. Statistical significance was tested using repeated two-way ANOVA with Bonferroni post hoc test. **, $p < 0.01$; ***, $p < 0.001$; *ns*, not significant.

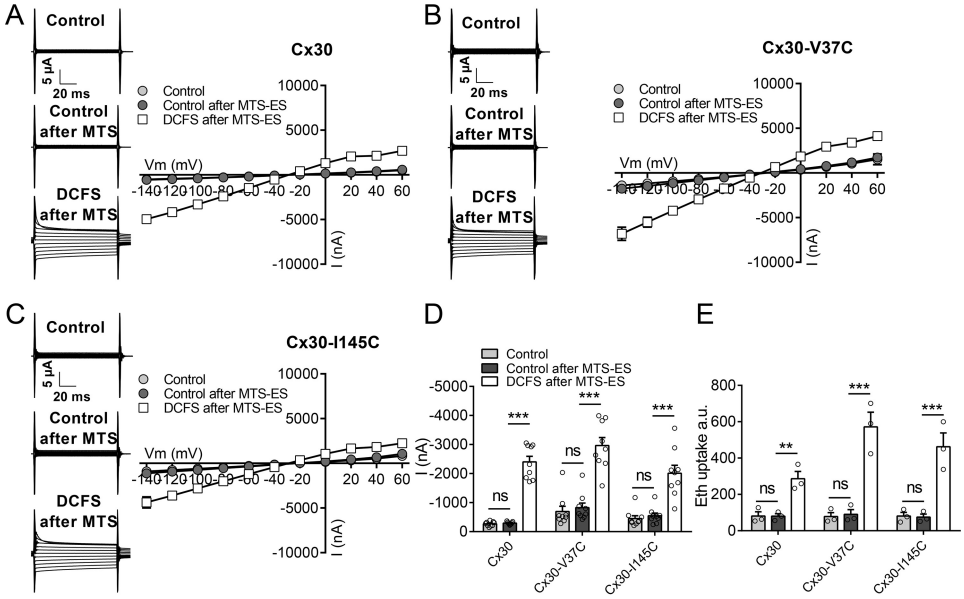

Figure 7. Effect of MTS-ES on Cx30, Cx30-V37C, and Cx30-I145C hemichannel activity. *A–C*, the effect of 1-min exposure to MTS-ES in control solution on the membrane currents was determined for Cx30 (*A*, $n = 9$), Cx30-V37C (*B*, $n = 9$), and Cx30-I145C (*C*, $n = 9$) hemichannels. The experiments were performed as described in Fig. 6. Representative current traces are shown in the *left panels*, and I/V summaries of $n = 9$ are shown in the *right panels*. *D*, histogram of all membrane currents obtained at −80 mV. *E*, ethidium (*Eth*) uptake recorded after 1-h exposure to control solution or DCFS after 5 min pretreatment in control solution or control solution containing 2 mM MTS-ES ($n = 3$ for all conditions). Data in I/V curves and in the bar graphs are presented as mean ± S.E. The individual data points are shown by overlaid scatterplots in bar graphs. Statistical significance was tested using repeated two-way ANOVA with Bonferroni post hoc test. **, $p < 0.01$; ***, $p < 0.001$; *ns*, not significant.

release of microinjected radioactively labeled ATP in Cx30-expressing oocytes (20), which may be a more sensitive approach than the luciferase assay. However, this lack of detectable DCFS-mediated ATP release, despite parallel demonstration of conductance and dye uptake in batch-matched oocytes, indicates that the Cx30 hemichannel–mediated ATP release is quantitatively minor compared with conductance and dye flux. It certainly reinforces the point that the latter should not be used to infer the former for any connexin channel. It remains possible that connexin-dependent ATP release from some cell types/under certain experimental conditions may not occur directly via the hemichannel pore.

Differential regulation of the permeability of ionic currents and larger molecules (*i.e.* fluorescent probes, purines, etc.) have been described for connexin channels in the gap junctional configuration (3, 4, 6, 7, 11, 29, 52–54). A possible explanation for the differences in relative permeabilities may link to the existence of different channel substates. Along these lines, Kwak *et al.* (29) showed that PKC activation increased electrical coupling while reducing intercellular dye transfer (29). This change was associated with a relative shift from large to small single-channel events, suggesting that only the larger conductance states permitted dye diffusion. These findings were supported by later studies of current *versus* permeability in relation to phosphorylation (11) and voltage-gating (52). Although such a mechanism may explain some scenarios, including the differential gating seen here, others remain unaccounted for (*e.g.* dye permeation in Cx36 and Cx43 hemichannels in the absence of current under similar experimental conditions (28)).

For both gap-junctional and hemichannel configurations, the underlying molecular pore-lining structural determinants of the permeation profile have remained elusive. Some guidance has been provided by the 3.5-Å structure of Cx26 (37, 47), but at this relatively low resolution, the specific positions of amino acid side chains within the pore rely predominantly on modeling. Direct empirical probing of the pore has been performed on both gap junction and hemichannel configurations by SCAM, where pore-lining residues are individually mutated to cysteine and tested for accessibility to aqueously soluble thiol regents by assaying for changes in channel conductance. These analyses have yielded quite distinct patterns of reactivity when conducted on hemichannel and gap junction configurations, with the former implicating M1, and the latter M3 and part of M2, as pore lining (35, 36, 38, 39, 41, 42). The X-ray structure supports the M1 assignment, consistent with the crystal likely being derived from solubilized hemichannels.

In an attempt to probe residues that might differentially influence dye and ionic permeation, we conducted SCAM analyses on six Cx30 residues: Val-37 (M1 pore-lining in the Cx26 crystal structure (37) and involved in KID and Clouston syndromes when mutated to a glutamate in Cx30 (55, 56)), Glu-42 (E1 pore-lining in Cx46 and Cx50 hemichannels (35, 38–40)), and Val-84 (M2), Tyr-136, Ile-145, and Phe-150 (M3), all pore-lining in Cx32 and Cx50 gap junctions (36, 42). Unfortunately, the comprehensive view these sites could have provided were limited by the fact that only two of the cysteine substitutions formed functional hemichannels (Cx30-V37C and Cx30-I145C), comparable with that of the WTCx30. Although the negatively charged thiol, MTS-ES, had no effect on either mutant, the positively charged MTS-ET caused an increase in the Cx30-V37C–mediated membrane currents with no impact on ethidium uptake. This differential effect on the two permeants underscores that the pore is discriminating and that ethidium permeability cannot be used to infer permeability to other molecules, even ions, or vice versa. This finding demonstrates that the positively charged thiol agent is able to gain entrance into the pore of Cx30 hemichannels even in the presence of 1 mM divalent cations. It also represents the first empirical validation of Val-37 as a hemichannel pore-lining residue, as seen in the X-ray structure. The failure of the Ile-145 site to react is consistent with the M1 lining the pore in the hemichannel configuration, where M3 is inaccessible (in contrast to the gap junction configuration). Two critical questions are why reaction of MTS-ET caused an increase in conductance, rather than a block of the channel (as seen in most SCAM studies), and why this differentially affected conductance and ethidium permeation. It is possible that reaction at this site induced a conformational change that might differentially affect small ion and ethidium permeability. However, reaction with the thiol did not interfere with the regular function of the Cx30 hemichannel, as removal of divalent cations caused the usual increase in both ethidium uptake and membrane current. One alternative is that the channels are wide enough that reaction with a single MTS-ET was not sufficient to occlude the channel but that the introduced positive charge may have enhanced the anionic conductance of the pore without significantly diminishing cationic fluorescence transfer. A similar differential MTS-dependent effect on the transport of ions and small fluorescent dyes was reported previously for Cx46 hemichannels (38). The addition of thiol reagents in the presence of 1 mM Ca^{2+} may offer some insights into why there was a difference in the effects of positive and negatively changed MTS reagents. Modeling studies on Cx26 indicate that an electrostatic network, serving to coordinate a Ca^{2+}-gating ring, may be located near the entrance of the connexin pore, stabilizing the closed form of the hemichannel at physiological Ca^{2+} concentrations (50). This Ca^{2+} ring may serve as an electrostatic barrier to larger anions like MTS-ES, although it is unclear why it would not pose a barrier to MTS-ET. Perhaps more likely is the possibility that the strong positive potentials proposed to line the entire pore in the Ca^{2+}-bound state (47) may bind larger anions and limit their availability for reaction with exposed thiols.

In conclusion, the distinct and selective permeability of individual connexin hemichannels may serve a physiological function. Although Cx30-mediated hemichannel activity could be beneficial in certain settings (57), one can well imagine that the Cx43-expressing myocardium would be compromised by opening of large-pore, non-selective ion channels. This study demonstrates, however, that, under narrow ranges of extracellular divalent cations, one can prevent leak of larger molecules while still allowing low levels of ionic conductance. This may be of particular importance for Cx30 in the ear, where it is exposed to a wide range of different extracellular Ca^{2+} concentrations. This could be amplified further if the larger molecules were of different charge, as would be the case for molecules such as ATP. Thus, connexin-specific gating and permeability characteristics (both in gap junction and hemichannel configurations) may provide cells with the molecular means to differentially control its membrane permeability and intercellular communication based on the connexin isoform expressed and the specific sensitivities to gating signals like divalent cations.

Materials and methods

In vitro transcription

cDNA encoding mouse Cx30 (mCx30, obtained from Klaus Willecke, Bonn University) was subcloned into the expression vector pXOOM, and its sequence was verified. Point mutations

were introduced into Cx30 by the QuikChange site-directed mutagenesis kit (Stratagene, Santa Clara, CA) and verified by DNA sequencing. The cDNAs encoding WT and mutant versions of Cx30 were linearized downstream from the poly(A) segment and subsequently transcribed with T7 mMessage Machine according to the instructions of the manufacturer (Ambion, Austin, TX). The cRNA was extracted with MEGAclear (Ambion) prior to microinjection into defolliculated *X. laevis* oocytes (10 ng of RNA/oocyte).

Oocyte preparation

Oocytes were surgically removed from *X. laevis* frogs (Nasco or National Center for Scientific Research) according to European Community guidelines for the use of experimental animals and under a license issued for the use of experimental animals by the Danish Ministry of Justice (Dyreforsøgstilsynet). The oocytes were prepared as described previously (58) and kept for ~24 h at 18 °C in Kulori medium (90 mM NaCl, 1 mM KCl, 1 mM $MgCl_2$, 1 mM $CaCl_2$, 5 mM HEPES, and ~4 mM Tris $(HOCH_2)_3CNH_2$ (pH 7.4)) prior to cRNA injection. The microinjected oocytes were kept in Kulori medium at 18 °C for 2–4 days before the experiments were performed (except for ATP release in Cx30-D50N–expressing oocytes, which was carried out <24 h after microinjection). XeCx38 has been reported previously to be expressed by *Xenopus* oocytes (59, 60) although we have been unable to detect any Ca^{2+}- or Gd^{3+}-sensitive dye uptake or current in uninjected control oocytes under our experimental conditions (regardless of whether siRNA targeting Cx38 was microinjected into the oocytes (20, 45)). Cx38, at its endogenous expression level, is therefore unlikely to interfere with our data on the over-expressed Cx30.

Solutions

The control solution contained 100 mM NaCl, 2 mM KCl, 1 mM $CaCl_2$, 1 mM $MgCl_2$, 10 mM HEPES, and ~4 mM Tris ($(HOCH_2)_3CNH_2$) (pH 7.4). Solutions depleted for one or both divalent cations used equiosmolar NaCl. Specifically, MgFS contained 101.5 mM NaCl, 2 mM KCl, 1 mM $CaCl_2$, 10 mM HEPES, and ~4 mM Tris (pH 7.4). CaFS contained 101.5 mM NaCl, 2 mM KCl, 1 mM $MgCl_2$, 10 mM HEPES, and ~4 mM Tris (pH 7.4). DCFS contained 103 mM NaCl, 2 mM KCl, 10 mM HEPES, and ~4 mM Tris (pH 7.4). The solutions employed for the Ca^{2+} and Mg^{2+} inhibition curves were obtained by diluting solutions containing 5 mM of either Ca^{2+} or Mg^{2+} (95.5 mM NaCl, 2 mM KCl, 5 mM $CaCl_2$/$MgCl_2$, 10 mM HEPES, and ~4 Tris (pH 7.4) with an equiosmolar divalent cation–free solution.

Electrophysiology

The two-electrode voltage clamp recordings were performed at room temperature with a Dagan Clampator interfaced to a personal computer with a Digidata 1320 A/D converter and pCLAMP 9.2 (both Axon instruments, Molecular Devices, CA. Electrodes were pulled from borosilicate glass capillaries to a resistance of 1–4 megaohm when filled with 1 M KCl. Currents were low-pass-filtered at 500 Hz and sampled at 2 kHz. Current/voltage (I/V) curves were obtained from the steady-state current levels and recorded in control solution or after 60-s exposure to a test solution from a holding potential of −30 or −50 mV by application of 100- to 200-ms voltage steps from +60 to −140 mV in increments of 20 mV, as indicated in the figure legends.

Ethidium uptake

The ethidium uptake was performed essentially as described earlier (61), with six oocytes per experimental condition. In brief, oocytes were washed in the relevant test solution and subsequently agitated mildly at room temperature in 500 μl of test solution with 50 μM ethidium bromide for 1 h. We have shown previously that ethidium uptake is a linear function of time within this time frame (20, 61). The oocytes were washed twice in control solution, individually lysed in 50 μl of distilled H_2O, and the fluorescence was determined with a Synergy HD plate reader (BioTek) and Gen5 software (BioTek) with 340/11 nm and 590/35 nm filters for excitation and emission, respectively. The obtained fluorescence is given in arbitrary units or normalized.

ATP release

The oocytes (six per condition) were washed in the relevant test solution and then incubated in 250 μl of the same test solution at room temperature. After 1 h, 10 μl of each experimental solution was collected and assayed according to the ATP determination kit protocol (Molecular Probes, A22066). The bioluminescence was determined with a Synergy HD plate reader (BioTek) and Gen5 software (BioTek) prior to subtraction of background luminescence. The ATP concentration was calculated from the standard curve obtained in parallel with each experiment.

Membrane purification and Western blotting

Purified plasma membranes were obtained from oocytes expressing the mutant constructs (10 oocytes of each), as described in detail previously (44). Briefly, to obtain the pure plasma membrane fraction, the oocyte vitelline envelope was partly digested with subtilisin A and subsequently polymerized to the plasma membrane with Ludox and polyacrylic acid (all from Sigma-Aldrich). The oocytes were homogenized and, following a series of centrifugation steps in the presence of proteinase inhibitors, the pure fraction of plasma membrane/vitelline envelope leaflets was obtained. The samples were analyzed by SDS-PAGE (12% precast gels) and Western blotting using anti-Cx30 (1:125, Invitrogen, 71-2200), followed by anti-rabbit HRP secondary antibody (1:3000, Bio-Rad, 170-6515). Protein staining was visualized by chemiluminescence (SuperSignal West Pico, Thermo Scientific; BioSpectrumAC Imaging System, UVP) and quantification in the linear range of exposure.

Chemicals

Gd^{3+} (50 μM final concentration, 100 mM stock in H_2O) and ethidium bromide (50 μM final concentration, 25 mM stock in H_2O) were obtained from Sigma-Aldrich. [2-(trimethylammonium)ethyl] methane thiosulfonate bromide (MTS-ET) and sodium (2-sulfonatoethyl) methane thiosulfonate (MTS-ES) were from Anatrace (Kem-En-Tec Nordic). Aliquots of dry

MTS-ES and MTS-ET powder were placed in small tubes and stored at −20 °C. On the day of use, the powder was dissolved in water to a stock concentration of 200 mM and kept on ice for a maximum of 4 h before it was further dissolved in the test solution to a concentration of 2 mM maximum 3 min before use.

Statistics

All experiments were performed with oocytes from at least three different animal donors. For ethidium uptake experiments, *n* refers to the number of experiments (each carried out with six oocytes per experimental condition). For electrophysiological experiments, *n* refers to the number of oocytes. Inhibition curves were fitted in GraphPad Prism 6.0 according to the equation $Y = 100 / (1 + 10\text{^}((\log IC_{50} - X) \times \text{Hill slope}))$, where X is the logarithm of the concentration. Statistical analysis was performed with GraphPad Prism 5–7, and the applied statistical test is indicated in the figure legends. Data are expressed as averages ± S.E., and $p < 0.05$ is considered statistically significant

Author contributions—N. M., J. S. A., and B. N. contributed to the research design. J. S. A. and B. S. N. conducted the experiments, analyzed the data, and prepared the figures. N. M., J. S. A., B. S. N., M. S. N., and N. M. contributed to the interpretation and discussion of the data. J. S. A., B. S. N., M. S. N., B. N., and N. M. contributed to drafting the article and approved the final version of the manuscript.

Acknowledgments—We thank Klaus Willecke (Bonn University) for providing the Cx30 cDNA and Charlotte G. Iversen and Mette Assentoft for expert technical assistance.

References

1. Nielsen, M. S., Axelsen, L. N., Sorgen, P. L., Verma, V., Delmar, M., and Holstein-Rathlou, N.-H. (2012) Gap junctions. *Compr. Physiol.* **2,** 1981–2035
2. Söhl, G., and Willecke, K. (2003) An update on connexin genes and their nomenclature in mouse and man. *Cell Commun. Adhes.* **10,** 173–180
3. Harris, A. L. (2007) Connexin channel permeability to cytoplasmic molecules. *Prog. Biophys. Mol. Biol.* **94,** 120–143
4. Nicholson, B. J., Weber, P. A., Cao, F., Chang, H., Lampe, P., and Goldberg, G. (2000) The molecular basis of selective permeability of connexins is complex and includes both size and charge. *Braz. J. Med. Biol. Res. Rev.* **33,** 369–378
5. Oviedo-Orta, E., and Howard Evans, W. (2004) Gap junctions and connexin-mediated communication in the immune system. *Biochim. Biophys. Acta.* **1662,** 102–112
6. Goldberg, G. S., Moreno, A. P., and Lampe, P. D. (2002) Gap junctions between cells expressing connexin 43 or 32 show inverse permselectivity to adenosine and ATP. *J. Biol. Chem.* **277,** 36725–36730
7. Goldberg, G. S., Lampe, P. D., and Nicholson, B. J. (1999) Selective transfer of endogenous metabolites through gap junctions composed of different connexins. *Nat. Cell Biol.* **1,** 457–459
8. Niessen, H., Harz, H., Bedner, P., Krämer, K., and Willecke, K. (2000) Selective permeability of different connexin channels to the second messenger inositol 1,4,5-trisphosphate. *J. Cell Sci.* **113**, 1365–1372
9. Ek-Vitorin, J. F., and Burt, J. M. (2013) Structural basis for the selective permeability of channels made of communicating junction proteins. *Biochim. Biophys. Acta* **1828,** 51–68
10. Goldberg, G. S., Valiunas, V., and Brink, P. R. (2004) Selective permeability of gap junction channels. *Biochim. Biophys. Acta* **1662,** 96–101
11. Ek-Vitorin, J. F., King, T. J., Heyman, N. S., Lampe, P. D., and Burt, J. M. (2006) Selectivity of connexin 43 channels is regulated through protein kinase C-dependent phosphorylation. *Circ. Res.* **98,** 1498–1505
12. Ye, Z.-C., Wyeth, M. S., Baltan-Tekkok, S., and Ransom, B. R. (2003) Functional hemichannels in astrocytes: a novel mechanism of glutamate release. *J. Neurosci.* **23,** 3588–3596
13. Sánchez, H. A., Mese, G., Srinivas, M., White, T. W., and Verselis, V. K. (2010) Differentially altered Ca^{2+} regulation and Ca^{2+} permeability in Cx26 hemichannels formed by the A40V and G45E mutations that cause keratitis ichthyosis deafness syndrome. *J. Gen. Physiol.* **136,** 47–62
14. Orellana, J. A., Díaz, E., Schalper, K. A., Vargas, A. A., Bennett, M. V., and Sáez, J. C. (2011) Cation permeation through connexin 43 hemichannels is cooperative, competitive and saturable with parameters depending on the permeant species. *Biochem. Biophys. Res. Commun.* **409,** 603–609
15. Stout, C. E., Costantin, J. L., Naus, C. C., and Charles, A. C. (2002) Intercellular calcium signaling in astrocytes via ATP release through connexin hemichannels. *J. Biol. Chem.* **277,** 10482–10488
16. Contreras, J. E., Sánchez, H. A., Eugenin, E. A., Speidel, D., Theis, M., Willecke, K., Bukauskas, F. F., Bennett, M. V., and Sáez, J. C. (2002) Metabolic inhibition induces opening of unapposed connexin 43 gap junction hemichannels and reduces gap junctional communication in cortical astrocytes in culture. *Proc. Natl. Acad. Sci. U.S.A.* **99,** 495–500
17. Ramachandran, S., Xie, L.-H., John, S. A., Subramaniam, S., and Lal, R. (2007) A novel role for connexin hemichannel in oxidative stress and smoking-induced cell injury. *PLoS ONE* **2,** e712
18. John, S. A., Kondo, R., Wang, S. Y., Goldhaber, J. I., and Weiss, J. N. (1999) Connexin-43 hemichannels opened by metabolic inhibition. *J. Biol. Chem.* **274,** 236–240
19. Valiunas, V., and Weingart, R. (2000) Electrical properties of gap junction hemichannels identified in transfected HeLa cells. *Pflugers Arch.* **440,** 366–379
20. Hansen, D. B., Braunstein, T. H., Nielsen, M. S., and MacAulay, N. (2014) Distinct permeation profiles of the connexin 30 and 43 hemichannels. *FEBS Lett.* **588,** 1446–1457
21. Cherian, P. P., Siller-Jackson, A. J., Gu, S., Wang, X., Bonewald, L. F., Sprague, E., and Jiang, J. X. (2005) Mechanical strain opens connexin 43 hemichannels in osteocytes: a novel mechanism for the release of prostaglandin. *Mol. Biol. Cell.* **16,** 3100–3106
22. Bao, L., Sachs, F., and Dahl, G. (2004) Connexins are mechanosensitive. *Am. J. Physiol. Cell Physiol.* **287,** C1389–C1395
23. Froger, N., Orellana, J. A., Calvo, C.-F., Amigou, E., Kozoriz, M. G., Naus, C. C., Sáez, J. C., and Giaume, C. (2010) Inhibition of cytokine-induced connexin43 hemichannel activity in astrocytes is neuroprotective. *Mol. Cell. Neurosci.* **45,** 37–46
24. Garré, J. M., Retamal, M. A., Cassina, P., Barbeito, L., Bukauskas, F. F., Sáez, J. C., Bennett, M. V., and Abudara, V. (2010) FGF-1 induces ATP release from spinal astrocytes in culture and opens pannexin and connexin hemichannels. *Proc. Natl. Acad. Sci. U.S.A.* **107,** 22659–22664
25. Sáez, J. C., Schalper, K. A., Retamal, M. A., Orellana, J. A., Shoji, K. F., and Bennett, M. V. (2010) Cell membrane permeabilization via connexin hemichannels in living and dying cells. *Exp. Cell Res.* **316,** 2377–2389
26. Abbaci, M., Barberi-Heyob, M., Blondel, W., Guillemin, F., and Didelon, J. (2008) Advantages and limitations of commonly used methods to assay the molecular permeability of gap junctional intercellular communication. *BioTechniques* **45,** 33–52, 56–62
27. Bahima, L., Aleu, J., Elias, M., Martín-Satué, M., Muhaisen, A., Blasi, J., Marsal, J., and Solsona, C. (2006) Endogenous hemichannels play a role in the release of ATP from *Xenopus* oocytes. *J. Cell. Physiol.* **206,** 95–102
28. Hansen, D. B., Ye, Z.-C., Calloe, K., Braunstein, T. H., Hofgaard, J. P., Ransom, B. R., Nielsen, M. S., and MacAulay, N. (2014) Activation, permeability, and inhibition of astrocytic and neuronal large pore (hemi-)channels. *J. Biol. Chem.* **289,** 26058–26073
29. Kwak, B. R., van Veen, T. A., Analbers, L. J., and Jongsma, H. J. (1995) TPA increases conductance but decreases permeability in neonatal rat cardiomyocyte gap junction channels. *Exp. Cell Res.* **220,** 456–463
30. Vavrusova, M., and Skibsted, L. H. (2013) Calcium binding to dipeptides of aspartate and glutamate in comparison with orthophosphoserine. *J. Agric. Food Chem.* **61,** 5380–5384
31. Lee, J. R., Derosa, A. M., and White, T. W. (2009) Connexin mutations causing skin disease and deafness increase hemichannel activity and cell

death when expressed in *Xenopus* oocytes. *J. Invest. Dermatol.* **129,** 870–878
32. Sanchez, H. A., Villone, K., Srinivas, M., and Verselis, V. K. (2013) The D50N mutation and syndromic deafness: altered Cx26 hemichannel properties caused by effects on the pore and intersubunit interactions. *J. Gen. Physiol.* **142,** 3–22
33. González, D., Gómez-Hernández, J. M., and Barrio, L. C. (2006) Species specificity of mammalian connexin-26 to form open voltage-gated hemichannels. *FASEB J.* **20,** 2329–2338
34. Gómez-Hernández, J. M., de Miguel, M., Larrosa, B., González, D., and Barrio, L. C. (2003) Molecular basis of calcium regulation in connexin-32 hemichannels. *Proc. Natl. Acad. Sci. U.S.A.* **100,** 16030–16035
35. Kronengold, J., Trexler, E. B., Bukauskas, F. F., Bargiello, T. A., and Verselis, V. K. (2003) Single-channel SCAM identifies pore-lining residues in the first extracellular loop and first transmembrane domains of Cx46 hemichannels. *J. Gen. Physiol.* **122,** 389–405
36. Skerrett, I. M., Aronowitz, J., Shin, J. H., Cymes, G., Kasperek, E., Cao, F. L., and Nicholson, B. J. (2002) Identification of amino acid residues lining the pore of a gap junction channel. *J. Cell Biol.* **159,** 349–360
37. Maeda, S., Nakagawa, S., Suga, M., Yamashita, E., Oshima, A., Fujiyoshi, Y., and Tsukihara, T. (2009) Structure of the connexin 26 gap junction channel at 3.5 A resolution. *Nature* **458,** 597–602
38. Zhou, X. W., Pfahnl, A., Werner, R., Hudder, A., Llanes, A., Luebke, A., and Dahl, G. (1997) Identification of a pore lining segment in gap junction hemichannels. *Biophys. J.* **72,** 1946–1953
39. Kronengold, J., Srinivas, M., and Verselis, V. K. (2012) The N-terminal half of the connexin protein contains the core elements of the pore and voltage gates. *J. Membr. Biol.* **245,** 453–463
40. Verselis, V. K., Trelles, M. P., Rubinos, C., Bargiello, T. A., and Srinivas, M. (2009) Loop gating of connexin hemichannels involves movement of pore-lining residues in the first extracellular loop domain. *J. Biol. Chem.* **284,** 4484–4493
41. Tang, Q., Dowd, T. L., Verselis, V. K., and Bargiello, T. A. (2009) Conformational changes in a pore-forming region underlie voltage-dependent "loop gating" of an unapposed connexin hemichannel. *J. Gen. Physiol.* **133,** 555–570
42. Toloue, M. M. (2007) *Selectivity of Gap Junctions for Natural Metabolites and Its Structural Basis.* Ph.D. Thesis, University of Buffalo
43. Iglesias, R., Dahl, G., Qiu, F., Spray, D. C., and Scemes, E. (2009) Pannexin 1: the molecular substrate of astrocyte "hemichannels." *J. Neurosci.* **29,** 7092–7097
44. Moeller, H. B., MacAulay, N., Knepper, M. A., and Fenton, R. A. (2009) Role of multiple phosphorylation sites in the COOH-terminal tail of aquaporin-2 for water transport: evidence against channel gating. *Am. J. Physiol. Renal Physiol.* **296,** F649–F657
45. Nielsen, B. S., Hansen, D. B., Ransom, B. R., Nielsen, M. S., and MacAulay, N. (2017) Connexin hemichannels in astrocytes: an assessment of controversies regarding their functional characteristics. *Neurochem. Res.* 10.1007/s11064–017-2243–7
46. Lopez, W., Liu, Y., Harris, A. L., and Contreras, J. E. (2014) Divalent regulation and intersubunit interactions of human connexin26 (Cx26) hemichannels. *Channels* **8,** 1–4
47. Bennett, B. C., Purdy, M. D., Baker, K. A., Acharya, C., McIntire, W. E., Stevens, R. C., Zhang, Q., Harris, A. L., Abagyan, R., and Yeager, M. (2016) An electrostatic mechanism for Ca^{2+}-mediated regulation of gap junction channels. *Nat. Commun.* **7,** 8770
48. Lee, J. R., and White, T. W. (2009) Connexin-26 mutations in deafness and skin disease. *Expert Rev. Mol. Med.* **11,** e35
49. Lopez, W., Gonzalez, J., Liu, Y., Harris, A. L., and Contreras, J. E. (2013) Insights on the mechanisms of Ca^{2+} regulation of connexin26 hemichannels revealed by human pathogenic mutations (D50N/Y). *J. Gen. Physiol.* **142,** 23–35
50. Lopez, W., Ramachandran, J., Alsamarah, A., Luo, Y., Harris, A. L., and Contreras, J. E. (2016) Mechanism of gating by calcium in connexin hemichannels. *Proc. Natl. Acad. Sci. U.S.A.* **113,** E7986–E7995
51. Bone, L. J., Deschênes, S. M., Balice-Gordon, R. J., Fischbeck, K. H., and Scherer, S. S. (1997) Connexin32 and X-linked Charcot-Marie-Tooth disease. *Neurobiol. Dis.* **4,** 221–230
52. Bukauskas, F. F., Bukauskiene, A., and Verselis, V. K. (2002) Conductance and permeability of the residual state of connexin43 gap junction channels. *J. Gen. Physiol.* **119,** 171–185
53. Yum, S. W., Zhang, J., Valiunas, V., Kanaporis, G., Brink, P. R., White, T. W., and Scherer, S. S. (2007) Human connexin26 and connexin30 form functional heteromeric and heterotypic channels. *Am. J. Physiol. Cell Physiol.* **293,** C1032–C1048
54. Kanaporis, G., Brink, P. R., and Valiunas, V. (2011) Gap junction permeability: selectivity for anionic and cationic probes. *Am. J. Physiol. Cell Physiol.* **300,** C600–C609
55. Common, J. E., Becker, D., Di, W.-L., Leigh, I. M., O'Toole, E. A., and Kelsell, D. P. (2002) Functional studies of human skin disease- and deafness-associated connexin 30 mutations. *Biochem. Biophys. Res. Commun.* **298,** 651–656
56. Jan, A. Y., Amin, S., Ratajczak, P., Richard, G., and Sybert, V. P. (2004) Genetic heterogeneity of KID syndrome: identification of a Cx30 gene (GJB6) mutation in a patient with KID syndrome and congenital atrichia. *J. Invest. Dermatol.* **122,** 1108–1113
57. Anselmi, F., Hernandez, V. H., Crispino, G., Seydel, A., Ortolano, S., Roper, S. D., Kessaris, N., Richardson, W., Rickheit, G., Filippov, M. A., Monyer, H., and Mammano, F. (2008) ATP release through connexin hemichannels and gap junction transfer of second messengers propagate Ca^{2+} signals across the inner ear. *Proc. Natl. Acad. Sci. U.S.A.* **105,** 18770–18775
58. Fenton, R. A., Moeller, H. B., Zelenina, M., Snaebjornsson, M. T., Holen, T., and MacAulay, N. (2010) Differential water permeability and regulation of three aquaporin 4 isoforms. *Cell. Mol. Life Sci.* **67,** 829–840
59. Ebihara, L. (1996) Xenopus connexin38 forms hemi-gap-junctional channels in the nonjunctional plasma membrane of *Xenopus* oocytes. *Biophys. J.* **71,** 742–748
60. White, T. W., Bruzzone, R., Goodenough, D. A., and Paul, D. L. (1992) Mouse Cx50, a functional member of the connexin family of gap junction proteins, is the lens fiber protein MP70. *Mol. Biol. Cell.* **3,** 711–720
61. Alstrøm, J. S., Hansen, D. B., Nielsen, M. S., and MacAulay, N. (2015) Isoform-specific phosphorylation-dependent regulation of connexin hemichannels. *J. Neurophysiol.* **114,** 3014–3022